Modern Solar Facilities – Advanced Solar Science, 241–244
F. Kneer, K. G. Puschmann, A. D. Wittmann (eds.)
© Universitätsverlag Göttingen 2007

Modified p-modes in penumbral filaments

D. S. Bloomfield[1,*], A. Lagg[1], S. K. Solanki[1], and J. M. Borrero[2]

[1]Max-Planck-Institut für Sonnensystemforschung, Katlenburg-Lindau, Germany
[2]High Altitude Observatory, Boulder, Colorado, U.S.A.
[*]*Email:* bloomfield@mps.mpg.de

Abstract. A time series analysis was performed on velocity signals in a sunspot penumbra to search for possible wave modes. The spectropolarimetric photospheric data obtained by the Tenerife Infrared Polarimeter were inverted using the SPINOR code. An atmospheric model comprising two magnetic components and one stray-light component gave an optimal fit to the data. Fourier phase difference analysis between line-of-sight velocities of both magnetic components provided time delays between the two atmospheres. These delays were combined with the speeds of atmospheric wave modes and compared to height separations derived from velocity response functions to determine the wave mode.

1 Introduction

Disentangling the signatures of various magnetoatmospheric (MA) waves that are supported by magnetic atmospheres is a difficult, even daunting, task. However, information may be extracted from spatially unresolved structures by spectropolarimetry. This approach uses the full Stokes polarization spectra (I, Q, U, V), allowing physical properties of the emitting plasma to be inferred through the application of appropriate model atmospheres. Here we present a method that may identify the form of wave which exists in a magnetic environment.

2 Observations

Active region NOAA 10436 (Fig. 1) was observed on 21 August 2003 with the Tenerife Infrared Polarimeter (Martínez Pillet et al. 1999) attached to the German VTT. Full Stokes profiles were recorded for the spectral lines Fe I 15662.018 Å (effective Landé factor $\overline{g} = 1.50$) and Fe I 15665.245 Å ($\overline{g} = 0.75$) over the period 14:39-15:41 UT, yielding a time series of 250 stationary image positions on the slit at a cadence of one exposure every 14.75 s. Given the small amount of circular polarization asymmetry in the inner limbside penumbra, it is likely that these lines are not affected by gradients in the magnetic field vector or line-of-sight (LOS) velocity. Therefore, the data were inverted using the SPINOR inversion code (Frutiger 2000) and the height-independent two magnetic component model of Borrero et al. (2004). The inversion yields a magnetic field geometry consisting of a near-horizontal component (flux tube, FT) and a closer-to-vertical component (magnetic background, MB). Since the velocity variations were most strongly observed in Stokes Q the response functions (RFs) of Stokes Q to LOS velocity (Fig. 2) were calculated. The RFs of the magnetic components overlap over most part of the atmosphere, but their center-of-gravity (COG),

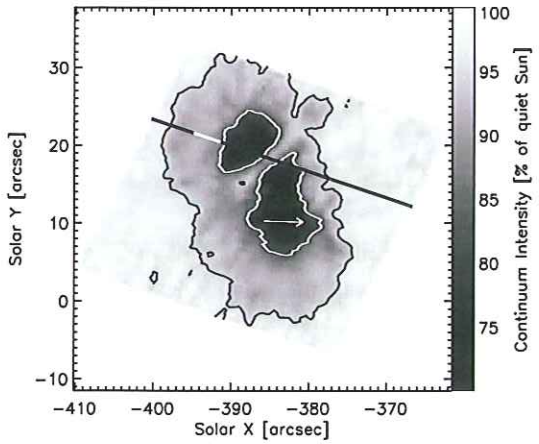

Figure 1. Continuum intensity image of NOAA 10436. White (black) contours mark the umbral/penumbral (penumbral/quiet Sun) boundaries. The straight black line marks the slit position during the time series, the white portion the region studied, while the arrow points to disk centre.

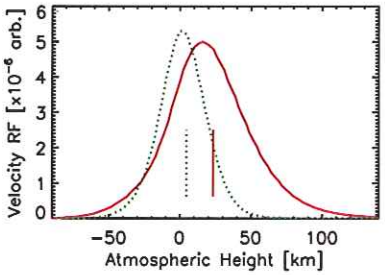

Figure 2. Height variation of combined 15662 Å and 15665 Å Stokes Q velocity response for the MB (solid) and FT (dotted) atmospheres. Vertical lines mark the COG in each component.

displayed as vertical lines, reveal a distinct separation between the components. Height differences between the LOS velocity signals were taken as the separation of the COGs, while wave propagation speeds were calculated over these height ranges from the output inversion atmospheres.

3 Time Series Analysis

A Fourier phase difference analysis was performed between the MB and FT velocity signals following Krijger et al. (2001). Spectra from the eleven analyzed pixels of the inner limb-side penumbra are overplotted in the left panel of Figure 3. Approximately constant phase difference values were recorded in the range 2.5 – 4.5 mHz, with the probability distribution function (PDF) centred on −5.5°. Negative phase differences mean that the FT velocity leads the MB, agreeing with the COG heights in Figure 2 for upward wave propagation. The centroid value was converted into time delay between the signals, resulting in values ranging

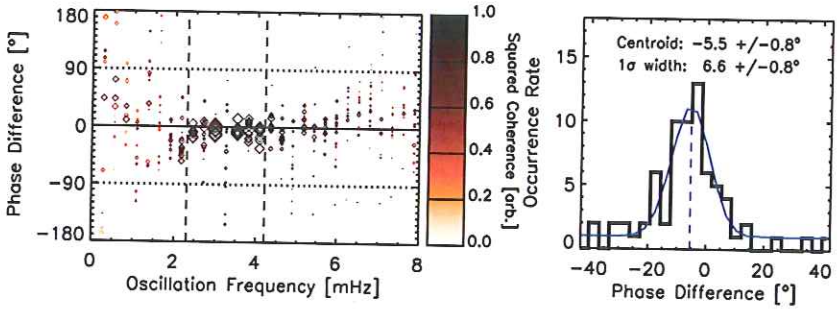

Figure 3. *Left*: Fourier phase difference spectra between the MB and FT velocities from the eleven analyzed pixels. Darker shading denotes greater Fourier coherence and larger symbol size greater cross-spectral power. *Right*: PDF of phase difference values over the frequency range 2.5 – 4.5 mHz. The thick curve displays the measured values and the thin curve the best-fit Gaussian profile.

from −6.3 s to −3.8 s. Attributing these phase differences to propagating waves conflicts with the evanescent behaviour of vertical waves below the acoustic cutoff (5.2 mHz). However, p-modes may travel at angles away from the vertical at these heights (e.g., 40° – 60° for l = 600 – 800 at 3.5 mHz; Cally 2006, private communication) and, for inclinations of 50°, frequencies $\geqslant$3.2 mHz may propagate.

4 Height Separation Comparison

The low-photospheric sampling of the spectral lines means that both components are mostly gas dominated (Fig. 2; $\beta \geqslant 1$ below 70 km and 90 km in the MB and FT, respectively). As such, differing forms of wave will have certain properties in terms of propagation speed and direction: acoustic waves propagate isotropically at the sound speed, c_S; Alfvén waves are restricted to the direction of the field and propagate at the Alfvén speed, v_A; MA slow modes propagate along the field at either v_A or the tube speed, c_T, if the sunspot is thought of as a large "flux tube"; MA fast modes propagate at a speed between c_S and $(c_S^2 + v_A)^{1/2}$ depending on the angle between the direction of the field and that of wave propagation.

Taking these considerations into account, the previously obtained vertical height separations are converted into path lengths along the direction of propagation: 50° to the vertical for acoustic and fast-mode waves; along the field for Alfvénic and slow-mode waves. Note that the fast-mode speed will differ between waves moving toward the sunspot (ingressing) and those moving away (egressing). Probability distribution functions of the RF-predicted path lengths are given as solid curves in Fig. 4, while values calculated by combining time delays, wave speeds and propagation angle to the field are overplotted as dotted and dashed curves. The best correspondence is observed for ingressing fast-mode waves: this case has the smallest difference between the RF-predicted and calculated path length COGs (Table 1).

5 Conclusions

This is the first time that spectropolarimetric data have been used in this manner to identify a MA wave mode. The fact that a fast-mode wave best fits the observational data makes

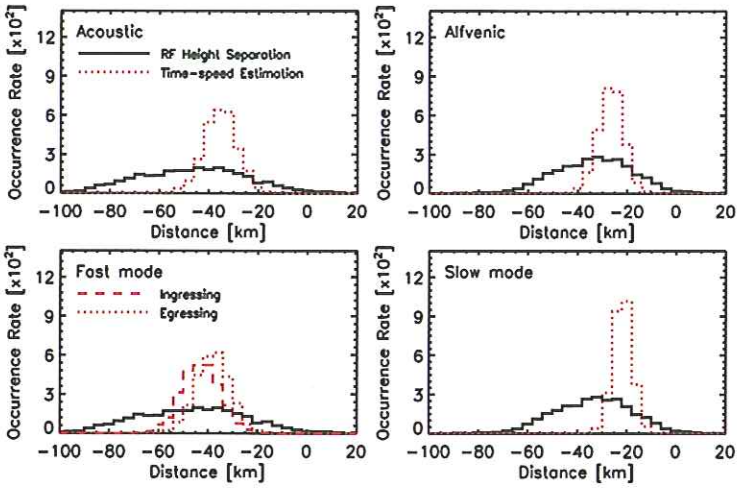

Figure 4. Comparison of RF-predicted (solid lines) and calculated (dotted and dahed lines) wave travel distances. Cases are presented for waves propagating at 50° to the vertical at the acoustic (*top left*) and fast-mode speeds (*bottom left*), as well as field-aligned waves propagating at the Alfvén (*top right*) and slow-mode tube speeds (*bottom right*). In all panels, vertical height separations were converted into path length along the direction of propagation.

Table 1. Differences between RF-predicted and calculated path length COG values.

Wave Type	Absolute Separations [km]
Acoustic	8
Alfvénic	4
Slow mode	9
Fast mode (ingressing)	0
Fast mode (egressing)	5

qualitative sense as the spectral lines sample a high-β region of the low photosphere where p-mode waves should be modified into a fast-mode form by the magnetic field. It will be interesting to see if the detected form of MA wave changes from the case where the velocity response of a spectral line is formed below $\beta = 1$ to one where it is formed above this level.

References

Borrero, J. M., Solanki, S. K., Bellot Rubio, L. R., Lagg, A., & Mathew, S. K. 2004, A&A, 422, 1093
Cally, P. S. 2006, private communication
Frutiger, C. 2000, Ph.D. Thesis, Institute of Astronomy, ETH, Zürich, No. 13896
Krijger, J. M., Rutten, R. J., Lites, B. W., Straus, Th., Shine, R. A., & Tarbell, T. D. 2001, A&A, 379, 1052
Martínez Pillet, V., et al. 1999, in High Resolution Solar Physics: Theory, Observations, and Techniques, ed. T. R. Rimmele, K. S. Balasubramaniam, & R. R. Radick, ASP Conf. Ser., 183, 264